Published in final edited form as:
*Phys Med Biol*. 2012 October 21; 57(20): 6571–6585. doi:10.1088/0031-9155/57/20/6571.

# Pulse Shape Discrimination and Classification Methods for Continuous Depth of Interaction Encoding PET Detectors

**Emilie Roncali**, **Jennifer E. Phipps**, **Laura Marcu**, and **Simon R. Cherry**
Department of Biomedical Engineering, University of California Davis, One Shields Avenue, Davis, CA 95616, USA

Emilie Roncali: eroncali@ucdavis.edu

## Abstract

In previous work we demonstrated the potential of positron emission tomography (PET) detectors with depth-of-interaction (DOI) encoding capability based on phosphor-coated crystals. A DOI resolution of 8 mm full-width at half-maximum was obtained for 20 mm long scintillator crystals using a delayed charge integration linear regression method (DCI-LR). Phosphor-coated crystals modify the pulse shape to allow continuous DOI information determination, but the relationship between pulse shape and DOI is complex. We are therefore interested in developing a sensitive and robust method to estimate the DOI. Here, linear discriminant analysis (LDA) was implemented to classify the events based on information extracted from the pulse shape. Pulses were acquired with $2 \times 2 \times 20$ mm$^3$ phosphor-coated crystals at five irradiation depths and characterized by their DCI values or Laguerre coefficients. These coefficients were obtained by expanding the pulses on a Laguerre basis set and constituted a unique signature for each pulse. The DOI of individual events was predicted using LDA based on Laguerre coefficients (Laguerre-LDA) or DCI values (DCI-LDA) as discriminant features. Predicted DOIs were compared to true irradiation depths. Laguerre-LDA showed higher sensitivity and accuracy than DCI-LDA and DCI-LR and was also more robust to predict the DOI of pulses with higher statistical noise due to low light levels (interaction depths further from the photodetector face). This indicates that Laguerre-LDA may be more suitable to DOI estimation in smaller crystals where lower collected light levels are expected. This novel approach is promising for calculating DOI using pulse shape discrimination in single-ended readout depth-encoding PET detectors.

### Keywords

Positron emission tomography (PET); Depth of interaction (DOI); Phosphor-coated scintillators; PET detectors; Laguerre expansion; Pulse shape discrimination; Linear discriminant analysis; Delayed Charge Integration (DCI)

## 1. Introduction

The need for excellent spatial resolution and sensitivity in small animal positron emission tomography (PET) motivated the initial development of depth of interaction (DOI) detectors for positron emission tomography. These detector designs are now being extended to clinical brain PET scanners where excellent spatial resolution and sensitivity also are required (de Jong *et al.*, 2007). Sensitivity improvements can be achieved by using thicker scintillator crystals and increasing the solid angle coverage. This can be accomplished by reducing the ring diameter to match the size of the subject; however this creates parallax errors that degrade the uniformity of the spatial resolution across the field of view (Moses and Derenzo, 1994). Incorporating DOI information in PET detectors reduces the parallax error, resulting

in scanners that can simultaneously have high and uniform spatial resolution as well as high sensitivity.

Various depth-encoding detector designs have been proposed. One method that has shown very good DOI resolution (~2 mm) with small scintillator arrays is the dual-ended readout method (Moses *et al.*, 1995; Yang *et al.*, 2008; St James *et al.*, 2009). This design provides continuous depth information and is very promising. However the increased complexity of the electronics as well as the doubling of the number of photodetectors increase cost and reduce practicality, especially for whole-body PET scanners. Approaches based on single-ended readout of the detector include multi-layer scintillator arrays with offset crystals, arrangements with light sharing between crystal layers providing discrete DOI information with a typical resolution of 5–10 mm (Tsuda *et al.*, 2004; Ito *et al.*, 2010), and monolithic scintillator PET detectors with DOI encoding (Maas *et al.*, 2009; Miyaoka *et al.*, 2010). It also includes phoswich detectors using scintillator layers with different decay times to encode DOI in a discrete manner with a resolution of 4 – 10 mm (Saoudi *et al.*, 1999; Seidel *et al.*, 1999; Eriksson *et al.*, 2009), depending on the thickness of the individual layers. Such detectors have now been integrated in commercially available preclinical scanners with a DOI resolution of 8 mm and improvement in spatial resolution has been demonstrated (Wang *et al.*, 2006). We aim to develop a detector based on single-ended readout that can achieve similar or better performance than the phoswich detector with a simpler and more cost effective design.

We have proposed an alternative DOI solution based on the use of phosphor-coated scintillation crystals (Du *et al.*, 2009). The phosphor absorbs and re-emits a fraction of the scintillation light and delays these converted photons due to the intrinsic decay time of the phosphor. By optimizing the coating along the crystal, the decay time of the detected pulses can be modified in a depth-dependent manner. Hence by recording and analysing the shape of pulses, the DOI can be extracted. Pulse-shape discrimination (PSD) methods allow for the extraction of features that can be used to calculate the DOI. In the case of phoswich detectors composed of several scintillator layers with distinct decay times, the DOI information is discrete and corresponds to the layer of interaction (Seidel *et al.*, 1999). Phosphor-coated crystals modify the pulse shape in a continuous manner, which allows the determination of continuous DOI information but also makes this calculation more complex.

In previous work, we showed that reasonable DOI resolution could be obtained with phosphor-coated crystals using the delayed charge integration (DCI) method (Du *et al.*, 2009). Pulses were integrated over a fixed window with and without a delay, and the ratio of those integrals provided the DCI value. For each individual pulse the DCI value was calculated and converted into a depth value to estimate the DOI of the event. This first step was performed using a linear regression between known irradiation depths and corresponding DCI values, and thus required a one-time calibration prior to DOI calculation. A DOI resolution of 8 mm full-width at half-maximum (FWHM) was obtained by this approach in 1.5 mm × 1.5 mm × 20 mm long scintillator crystals. Such a DOI resolution is not considered adequate for small-animal systems, as it would only permit segmentation of the crystal in to two or three DOI bins, which does not lead to sufficient improvement in spatial resolution uniformity. A more sophisticated post-processing approach should improve the estimation of DOI. The work presented in this paper explores different approaches to efficiently extract information from pulses generated in phosphor-coated crystals and process it to calculate the DOI of individual events.

Two main approaches can be taken to improve the accuracy of DOI information extracted from these scintillation crystals. First, the linear regression method previously used with DCI may be replaced by a classification task that sorts events into classes corresponding to

different depths of interaction. In this paper, we applied linear discriminant analysis (LDA) to classify the events based on information extracted from the pulse shape. Similar to the regression technique described above, a one-time acquisition of events at known irradiation depths is necessary to train the classifier. LDA can be performed with any independent features that characterize the pulses, with no additional computation time when using a combination of a large number of features.

Secondly, features other than DCI values as a function of depth may be used to describe the events generated in phosphor-coated crystals. DCI reduces the information contained in the shape of pulses to a single parameter, thus methods making use of the full waveform of the pulses may perform better in computing the DOI. This observation led us to use a Laguerre expansion technique to extract features of scintillation pulses in order to calculate their DOI by classification. This approach has been applied previously to identify various compounds via their fluorescence signature with time-resolved fluorescence spectroscopy (Marmarelis, 1993; Maarek *et al.*, 2000; Jo *et al.*, 2004). The Laguerre basis constitutes a family of functions that can be used to reconstruct signals without making any assumptions about the form of the signal to be reconstructed, in contrast to a typical multi-exponential fit. The Laguerre expansion makes use of the full waveform of recorded pulses by fitting them with a linear combination of Laguerre basis functions. These functions are orthonormal, ensuring a unique solution for the expansion of the signal. The resulting set of coefficients (namely Laguerre coefficients) constitutes a unique signature for each pulse and may be then used as discriminating features to classify individual light pulses using LDA (Phipps *et al.*, 2011).

The aims of the work described here are two-fold. We first investigated the potential of using LDA to classify events as a function of depth. To do so, pulses were acquired with single crystals at known irradiation depths. The DOI of individual events were then calculated by LDA with DCI values and compared to the depth obtained by DCI-based linear regression. We then studied how the classification performance was affected by using a Laguerre expansion to describe the pulse shapes instead of DCI. For this task, the same experimentally acquired pulses were used to calculate individual DOIs by LDA performed with Laguerre coefficients and compared to results obtained by LDA performed with DCI values. In the rest of the paper LDA performed with DCI values and LDA performed based on Laguerre expansion will be referred as DCI-LDA and Laguerre-LDA, respectively. Linear regression applied to DCI values will be referred as DCI-LR.

## 2. Materials & Methods

### 2.1. Experimental set-up

2 mm × 2 mm × 20 mm unpolished lutetium oxyorthosilicate (LSO) crystals (decay time ~ 40 nsecs) were coated with a $Y_3Al_5O_{12}$:Ce (YAG) phosphor (Comtech International Inc. Korea). The coating is a mixture of phosphor powder and optical cement NOA 88 (Norland Products, NJ). Both compounds are mixed to make a paste containing a concentration of 40% phosphor powder by weight that was applied on half the length of the crystal sides (furthest from photodetector) as well as the far end and then cured ~60 s with a UV lamp (Super Spot MK II, Lesco UV, CA). The coating thickness was ~0.25 mm. The decay time of the phosphor was measured to be 58 nsecs. YAG has an absorption peak at 430 nm that is a good match for the emission spectrum of LSO (which peaks at 420 nm), with an emission peak at 540 nm.

Crystals were wrapped in teflon tape and coupled to a single-channel photomultiplier tube (Hamamatsu R6231) using optical grease (BC-630, Bicron). The rise time of pulses from the PMT was ~3 ns. The detector, composed of the phosphor-coated LSO crystal coupled to the photomultiplier tube (PMT), was positioned in coincidence with a collimating detector

consisting of a 2 × 8 × 20 $mm^3$ block of LSO coupled to a single channel PMT (Hamamatsu R647). As shown in Figure 1, the orientation of the crystal in the collimating detector was chosen such that it was irradiated face-on, whereas the YAG-coated crystal was irradiated from the side by a 0.5 mm $^{22}Na$ point source of activity 3.7 MBq. The collimating detector together with the source was translated to irradiate the phosphor-coated crystal along its length at five different depths every four mm (2 mm away from the photodetector face, 6 mm, 10 mm, 14 mm and 18 mm) by using electronic coincidence to select events. The estimated width of the collimating beam at the crystal was 1.5 mm.

The signal from the R6231 PMT was passed through a fast amplifier (NIM Model 778, Philips Scientific, Ramsey, NJ) and recorded by an oscilloscope (Lecroy WavePro 7100). Signals from both PMTs were sent to constant fraction discriminators (CFD TC 453, Oxford Instruments Inc., Oak Ridge TN) and CFD signals were used to identify coincidence events with a quad-four fold logic unit (Model 756, Philips Scientific, Ramsey, NJ). The coincidence events were used to trigger the acquisition of ~1000 individual pulses at each depth with a sampling interval of 0.1 nsec for each pulse (sampling rate 10 GHz). Pulses were downsampled to a 1 GHz sampling rate before being processed.

### 2.2. DOI calculation by DCI-based linear regression (DCI-LR)

This method was applied in our previous work and was used here to serve as a reference. It was described in detail by Du *et al.*, 2009 and is summarized here. In this approach, each pulse is characterized by its DCI value (Seidel *et al.*, 1999; Chandrikamohan and DeVol, 2007). The signal, s(*t*), was integrated first over a window of width *W* and then a second time over a window of the same width *W*, but with a delay *D* (Figure 2). The DCI value is the ratio of those 2 integrals:

$$\text{DCI value}=\frac{\int_{t_0}^{t_0+W} s(t)dt}{\int_{t_0+D}^{t_0+D+W} s(t)dt} \quad (1)$$

This approach has two free parameters; the window width *W* and the delay *D*. Both are optimized to provide the largest variation of the DCI value between the two ends of the crystal (irradiation depths 2 mm and 18 mm) by maximizing the figure of merit (FOM) defined by Du *et al.*, 2009:

$$\text{FOM}=\frac{|\overline{DCI}_2-\overline{DCI}_{18}|}{\sigma(DCI_2)+\sigma(DCI_{18})} \quad (2)$$

where $\overline{DCI}_2$ and $\overline{DCI}_{18}$ are the mean DCI values at 2 and 18 mm and σ ($DCI_2$) and σ ($DCI_{18}$) are the standard deviation of the DCI values computed at those depths. The highest value for the FOM was found for $W$ = 130 ns and $D$=50 ns, so all DCI values were calculated with this set of parameters.

Data were partitioned in two groups of identical size (~2500 pulses per group). One group was used to perform the linear regression. To do so, for each of the five irradiation depths, the DCI values of pulses were histogrammed and the peaks of those histograms were plotted against the irradiation depth. A linear fit applied to this curve provided a model that allows DCI values to be converted into DOI (mm). The second group (~2500 pulses) was used to test the performance of the method. The model obtained by linear regression was used to predict DOIs of individual events of the second group. The predicted DOIs were then compared to the true irradiation depths which are known with a 1.5 mm precision (width of

the irradiation beam). This calibration is used routinely for DOI calculation with dual-ended readout detectors (Yang *et al.*, 2006).

### 2.3. Classification by Linear Discriminant Analysis

LDA is a classification technique originally developed by Fisher to separate data in two classes (Fisher, 1936). It was then extended to multi-class cases and is now widely used in pattern recognition and other applications (Krzanowski, 1988). LDA classifies observations into classes based on the information provided by a set of training data that describe the system; these data are used to train a classifier that can then be applied to predict to which class an observation belongs. The main assumption underlying LDA is that for each class the training data follow a multivariate normal distribution and that all classes have the same intra-class covariance. Only the means vary. LDA aims at separating groups of data by finding a new space in which both the separation and the compactness of classes are maximized (Li *et al.*, 2006). The separation and compactness are characterized by the inter-class covariance matrix $\hat{\Sigma}b$ and the intra-class covariance matrix $\hat{\Sigma}w$, respectively. Φ is the linear transform from the original space to the new space and can be obtained by solving the generalized eigenvalue problem:

$$\widehat{\Sigma}b\Phi=\lambda\widehat{\Sigma}w\Phi \quad (3)$$

where λ are the eigenvalues. This transformation is used to project observations to be classified in the new space. The Euclidean distances between an observation in the new space and the centroids are calculated; the observation is then assigned to the closest class.

Once again, data were partitioned in two groups: one group of pulses was used to train the LDA classifier whereas the second independent group was used to test the ability of the classification to predict DOIs of individual events. The crystal was virtually segmented in five equal depth bins centred on the irradiation depths. Those depth bins defined five classes labelled with the irradiation depth values (2, 6, 10, 14 and 18 mm) used in the classification.

### 2.4. Discriminating features for LDA: Laguerre expansion

In the case of phosphor-coated crystals, observations classified by LDA consisted of features extracted from the pulse shapes. Two types of features were investigated: DCI values and Laguerre coefficients. The DCI values were computed using Equation 1 with $W$ = 130 ns and $D$=50 ns. The calculation of Laguerre coefficients is detailed below.

**2.4.1 Laguerre expansion—**The recorded light pulses s($t$) are function of time $t$. s($t$) is composed of two terms: the response of the crystal x($t$) to a gamma interaction (fraction of light not changed by the phosphor) and x($t$) convolved with the response p($t$) of the phosphor coating (fraction of light modified by the phosphor).

$$s(t)=Kx(t)+(1-K)x(t)*p(t) \quad (4)$$

where * denotes the convolution operator and K the fraction of light not modified by the phosphor. Using the fact that the delta function δ($t$) is the identity for convolution (thus convolving a function by a delta function leaves the initial function unchanged) and that convolution is distributive, Equation 4 is equivalent to:

$$s(t)=x(t)*(K\delta(t)+(1-K)p(t)) \quad (5)$$

We define a function h($t$) = K δ($t$) + (1−K) p($t$) allowing s($t$) to be written as a simple convolution between x($t$) and h($t$):

$$s(t)=\int_0^t h(t')x(t-t')dt' \quad (6)$$

The scintillation decay $x(t)$ follows a single exponential with a time constant ~ 40 nsec (Melcher and Schweitzer, 1992). It was estimated from measured light pulses in a 2 × 2 × 20 $mm^3$ uncoated crystal (cut from the same LSO material used for the coated crystals) coupled to a PMT (as described in section 2.1). These measurements on an uncoated crystal also showed no depth dependence of the decay time, which allowed us to consider the decay time of the crystal response to be constant with depth in the absence of phosphor coating. The shape of the response due to the phosphor coating $h(t)$ varies with the depth of interaction, as the coating and the fraction of converted light (Equation 6) vary along the length of the crystal. $h(t)$ is therefore a function of time and depth of interaction.

Pulse signals $s(t)$ were digitalized by the oscilloscope with a time sampling $T$ of 1 ns with a total of $M$ time samples for each pulse. In this discrete-time case, the detected signal $s(n)$ can be expressed as (Maarek *et al.*, 2000; Jo *et al.*, 2004):

$$s(n)=T\sum_{m=0}^{M-1} h(m)x(n-m) \quad (7)$$

To deconvolve the crystal response $x(n)$ from the signal $s(n)$, the signal $h(m)$ was expanded on an ordered set of Laguerre basis functions such that:

$$h(m)=\sum_{i=0}^{I-1} Lc_i b_i(\alpha, m) \quad (8)$$

where $I$ is the order of expansion, $\alpha$ is the Laguerre parameter, $b_i$ the Laguerre basis functions and $Lc_i$ the Laguerre coefficients. The Laguerre basis functions $b_i$ are defined as:

$$b_i(\alpha, m)=\alpha^{m/2}(1-\alpha)^{1/2}\sum_{k=0}^{i}(-1)^k\binom{m}{k}\binom{i}{k}\alpha^{i-k}(1-\alpha)^k \quad (9)$$

The shape of the $b_i$ functions are specified by the Laguerre parameter $\alpha$, which varies between 0 and 1 and determines the rate of decline of the Laguerre functions. The order $i$ of a Laguerre function is equal to the number of zero-crossings of the function. An example of Laguerre basis functions calculated for an order of expansion $I = 8$ and $\alpha = 0.68$ is given in Figure 3.

Using Equation 7 and Equation 8, the estimated signal $\hat{s}(n)$ can be written as a linear combination of the functions $\nu_i(n)$:

$$\hat{s}(n)=\sum_{i=0}^{I-1} Lc_i \nu_i(\alpha, n) \quad (10)$$

where functions $\nu_i(n)$ are the Laguerre functions $b_i$ convolved with the scintillation signal $x(n)$:

$$v_i(n) = \sum_{m=0}^{M-1} b_i(\alpha, m) x(n-m) \quad (11)$$

For a given Laguerre basis set defined by α and *I*, the Laguerre expansion coefficients $Lc_i$ for a specific signal s(*n*) are estimated by solving the ordinary least square problem:

$$\underset{Lci \in R^I}{\text{minimize}} \; \| s(n) - \hat{s}(n) \|^2 \quad (12)$$

Solving Equation 12 provides a set of *I* Laguerre coefficients that gives the best fit ŝ(*n*) of the signal s(*n*). Laguerre coefficients reflect the contributions of the different Laguerre basis functions and do not have a physical meaning, but contain all the information about the shape of the pulse ŝ(*n*) and thus can be used to describe the signal s(*n*) in a given Laguerre basis set.

**2.4.2 Choosing α and I—**$\hat{s}(n)$ represents the fitted values of the signal s(*n*). The quality of the fit depends on the Laguerre basis set chosen to expand the signal s(*n*), so it is conditioned by the Laguerre parameter α and the order of expansion *I*. The quality of the fit was assessed by analysing the residuals between the signal s(*n*) and the estimated signal $\hat{s}(n)$ and was considered sufficient if the residuals contained only random noise and no unfitted component. This was measured by the $\chi^2$ statistic:

$$\chi^2 = \frac{1}{(N-I)\sigma^2} \sum_{n=0}^{N-1} (s(n) - \hat{s}(n))^2 \quad (13)$$

where $\sigma^2$ is the variance of the noise, *N* the number of time points and *I* the order of expansion. To estimate $\sigma^2$, the variance of all pulses of the training data was calculated at each time point, and plotted against the mean of those pulses at each time point on a logarithmic scale. The linear fit of this curve had a slope of 0.9, indicating that the signal was roughly Poisson and that the variance could reasonably be estimated by 1/ s(*n*) (Jo *et al.*, 2004).

The parameter pair (α, *I*) that minimizes $\chi^2$ was calculated for each pulse of the training data and the average values of α and *I* were found to be α = 0.68 and *I* = 8. This set of parameters defined the Laguerre basis set that was used to expand all pulses of the training group. The corresponding Laguerre coefficients were then used to train the LDA classifier. All pulses from the data group were also expanded on the same Laguerre basis set. Their set of Laguerre coefficients were used to predict their DOI by Laguerre-LDA.

## 2.5. Optimization of classification

The LDA technique applied to the DOI calculation of pulses generated in phosphor-coated crystals may be optimized by controlling several parameters. First, for Laguerre-LDA we ensured that the fitting of pulses via Laguerre expansion was optimal by selecting the Laguerre parameter α and the order of expansion *I* that provided the best fits, as described in the previous section. Secondly, for both DCI-LDA and Laguerre-LDA we investigated the effect of the size of the training group to ensure that enough pulses were used to train the classifier. To vary the size of the training group, 10 to 500 pulses per depth were randomly selected among pulses acquired at each irradiation depth. The DOI of pulses from the data group were then predicted by the classifier trained with each reduced training data group and the performance of the classification studied.

### 2.6. Evaluation of performance

For each depth bin, DOIs predicted by LDA were compared to the true depths of irradiation, first by histogramming the calculated DOIs at each irradiation depth (with five depth bins). Analysing results for individual depth bins enabled the assessment of performance of the classifier at different distances from the photodetector face. Two metrics were also used to better study the performance of the classification. First, the sensitivity per bin, defined as the ratio of correctly assigned events to the total number of events, and expressed as a percentage, was calculated for each depth bin. The sensitivity per bin characterizes the ability of the classifier to retrieve the depth of interaction on an event-by-event basis. Secondly, when pulses were not assigned to the correct bin, it was important to measure the error in positioning to evaluate the accuracy of the classifier. The error in positioning was computed for each bin as the average distance of events from their true irradiation depth (center of each bin). As opposed to LDA, linear regression does not assign a label (corresponding to the depth bin) to each event to be classified but computes a DOI value based on the DCI value of this event. To be able to compare results from DCI-LR to DCI-LDA and Laguerre-LDA, DOIs calculated by linear regression were assigned a label corresponding to the depth bin they belonged to (depth bins were the same as for LDA). This allowed the same metrics to be used across all methods.

## 3. Results

### 3.1. Variation of decay time as a function of irradiation depth

Example of individual pulses acquired at 2 mm and 18 mm from the photodetector is shown in Figure 4a. The variation of the decay times with depth was estimated by studying averaged pulses at each irradiation depth (Figure 4b). Averaged pulses were well described by a single exponential ($R^2$ values all > 0.99) and this was used to estimate the decay time variation along the crystal. The average decay time increased by 23 ns between depths of 2 mm and 18 mm. The largest variation is observed around 10 mm, where the phosphor coating starts. That sharp transition is reflected by a 10 ns increase between 6 mm and 10 mm and 7 ns between 10 mm and 14 mm. We anticipate that it will be more difficult to separate data between 14 and 18 mm since the decay time variation is only 2 ns. Averaged pulses were used only to observe trends in decay time variation with depth. All subsequent results were obtained by classification performed on individual pulses.

### 3.2. Training of the algorithms

**3.2.1 Effect of the training group size on LDA performance—**We studied the effect of the number of pulses per class used to train the algorithm by measuring the sensitivity and the positioning error averaged for all depth bins when classifying with training groups of different size. DCI-LDA and Laguerre-LDA were trained with groups which varied in size from 10 to 500 pulses per depth and then pulses from the data group were classified. As shown in Figure 5a, the sensitivity averaged for all bins increased when more pulses were used to train the classifier. For Laguerre-LDA, a rapid increase occurs initially and then the sensitivity plateaus when more than 250 pulses per depth bin are used. No significant change was observed with the DCI-LDA for training sets with more than 20 pulses per class.

A decrease in the positioning error was obtained for both classifications as the training set size increased, although there was no significant benefit for training sets with more than 100 pulses per depth bin (Figure 5b). Those results show that (i) the Laguerre-LDA is more sensitive to the training of the classifier than the DCI-LDA and (ii) that higher performance both in terms of sensitivity and positioning is obtained with the Laguerre-LDA.

**3.2.2 Linear regression—**DCI values calculated for individual pulses from the training group were histogrammed (Figure 6a). Histograms show the dispersion of DCI values at a given irradiation depth that will affect the DOI estimation using linear regression. This dispersion is partly due to the beam size (estimated to be ~ 1.5 mm in these experiments), and partly due to the statistical variations in detecting photons in the two charge integration windows. Figure 6a also shows that the difference between peak positions reaches a maximum between irradiation depths 6 mm and 10 mm and then decreases as the irradiation location moves further from the photodetector face, which indicates that the discrimination of pulses will be more difficult. The peak positions of the histograms were plotted against the known irradiation depth (Figure 6b) and fitted to derive a conversion function between the DCI value and the DOI in mm. A linear fit ($R^2$=0.9) was used to convert the DCI values in DOI in mm. The fitting error is much higher at depths >10 mm which suggests a poorer discrimination of DOIs between those depth bins.

### 3.3. Performance of classification

Classification used an independent set of pulses that were distinct from those used for training. DCI-LR showed lower performance than the two classification approaches at all depths except 2 mm and 14 mm, where performance was slightly higher (Figure 7 and Table 1). The error in positioning is lower than the DCI-LDA at depths 2, 10 and 14 mm and higher than the error obtained with Laguerre-LDA at all depths except 2 mm (Table 2).

Results of LDA classification performed with two different types of discriminating features are presented on Figure 7b-c (DCI-LDA and Laguerre-LDA, respectively). For each irradiation depth, DOI predicted by LDA were histogrammed. Histograms were normalized by the total number of events classified at each irradiation depth. Table 1 and Table 2 summarize the sensitivity and the positioning error for each bin. Figure 7b-c show that both classifications performed very well to predict DOIs of pulses acquired 2 mm away from the photodetector, as 75% of DOI of events were assigned correctly (Table 1). It is also important to note that the positioning error is small, as DOI not assessed correctly were almost all assigned to the neighbouring depth bin (6 mm). As a result, more than 97% of DOIs of pulses acquired at 2 mm were assigned to depth bins of 2 and 6 mm. At an irradiation depth of 6 mm, Laguerre-LDA performed slightly better than DCI-LDA with sensitivities of 54% and 52% and positioning errors of 2.2 mm and 2.3 mm (Table 1 and Table 2). For irradiation depths of 10 mm and 14 mm, Laguerre-LDA showed superior performance with higher sensitivities and lower positioning errors (Table 2). At 18 mm, more than 80% of DOI were assigned to either 18 mm or 14 mm bins with Laguerre-LDA. This was better than the DCI-LDA that assigned more pulses to 18 mm but mispositioned 15% of DOI at 10 mm. Considering all depths, Laguerre-LDA shows higher sensitivity and better accuracy in positioning than DCI-LDA, especially in the top half of the crystal (10 mm to 18 mm), furthest from the photodetector.

## 4. Discussion

The goal of this paper was to investigate the potential of linear discriminant analysis using Laguerre expansion to accurately estimate the DOI of individual events from phosphor-coated crystals. Overall, Laguerre-LDA showed better performance than DCI-LR used in previous work (Du *et al.*, 2009). Laguerre-LDA showed higher sensitivity (average sensitivity of 55% and 48%) and accuracy (average mispositioning of 2.4 mm and 3 mm) than DCI-LDA, demonstrating the potential of using the Laguerre expansion of the pulses.

It is important to note that the superiority of the Laguerre-LDA was most evident in the top half of the crystal (furthest from the photodetector) where the coating was applied. While DCI-LR performs slightly better than Laguerre-LDA at 2 mm and 14 mm, it performs

poorly at 10 mm and 18 mm where the depth bin with the most events is still at a depth of 14 mm. Figure 7a shows that DCI-LR has little discriminating power for events occurring in the top half of the crystal. In contrast, Laguerre-LDA assigns the most events to the correct depth bin, indicative of a better DOI resolution in the top half of the crystal. This is important, as in a scanner configuration the photodetector will be on the back side of the crystal and the majority of events occur towards the top of the crystal (larger distance from photodetector). Relatively few photons are reflected by the coated crystal sides; as a result, pulses from events occurring near the front of the crystal where the coating is applied are of lower amplitude and poorer statistical quality. The fact that Laguerre-LDA provides better performance at these depths suggests that it is more robust to statistical fluctuations coming from low light levels and therefore might be more suitable for smaller crystals.

The DOI classification performance mainly depends on the variation of decay times along the crystal and the variation of decay times within a given depth bin. Some in-bin dispersion will arise due to the finite width of the irradiating beam and the change in decay time over that width, however further and perhaps dominant dispersion in the measured values arises from statistical noise in the pulses due to the number of detected photons as well as the phosphor conversion efficiency. This indicates that Laguerre-LDA may be more suitable to DOI estimation in smaller crystals where lower light levels are expected. In addition, the value of the Laguerre expansion is that it makes full use of the waveform and is able to fit pulses very precisely. It may therefore benefit from a faster photodetector that would be sensitive to more variation in the pulses (especially the rise time), whereas the integration inherent to the DCI approach would not exploit such variations.

Linear regression strongly depends on the peak positions in the DCI histograms at different depths that give the calibration to convert DCI values to DOI in mm, as well as the FWHM at each depth. LDA classification has the advantage of being multi-dimensional and that different types of information from the events can be combined to refine the classification with no additional computation time. Indeed, Laguerre-LDA computation time depends primarily on two minimization problems (solving Equation 12 to compute the Laguerre coefficients and Equation 3 to perform LDA) that can be solved rapidly in matrix-vector form. Prior information could also be added to the classification. Other classification techniques could be used for the DOI calculation in this application. Other approaches implemented with phoswich detectors, such as fuzzy logic used for simultaneous beta/gamma spectroscopy (Yousefi and Lucchese, 2008) or neural networks applied to the detection of PET triple coincidences (Michaud *et al.*, 2010) may also be of interest.

Our future efforts are focused on working with a different photodetector with better QE in the yellow part of the spectrum (where the phosphor emits) and optimizing the coating scheme in order to improve the DOI resolution with the ultimate goal of developing a PET detector with single-ended readout and continuous DOI information. It also should be noted that the Laguerre expansion and the LDA methods explored here could be applied to other types of PET detectors based on continuous DOI information or pulse shape discrimination. This could help optimize the extraction of DOI information and lead to improved DOI resolution and thus uniformity of the spatial resolution across the field of view, to enhance the performance of PET scanners.

## Acknowledgments

This work was funded in part by grant DE-FG02-08ER85158 from the Department of Energy and by NIH grant CA134632. The authors want to thank Comtech Int. (Korea) for YAG powder samples as well as Andrea Ferrero and Julien Bec for useful discussions.

## References


Chandrikamohan P, DeVol TA. Comparison of pulse shape discrimination methods for phoswich and CsI:Tl detectors. IEEE Trans. Nucl. Sci. 2007; 54:398–403.

de Jong HWAM, van Velden FHP, Kloet RW, Buijs FL, Boellaard R, Lammertsma AA. Performance evaluation of the ECAT HRRT: an LSO-LYSO double layer high resolution, high sensitivity scanner. Phys. Med. Biol. 2007; 52:1505. [PubMed: 17301468]

Du H, Yang Y, Glodo J, Wu Y, Shah K, Cherry SR. Continuous depth-of-interaction encoding using phosphor-coated scintillators. Phys. Med. Biol. 2009; 54:1757–1771. [PubMed: 19258685]

Eriksson L, Melcher CL, Eriksson M, Rothfuss H, Grazioso R, Aykac M. Design considerations of phoswich detectors for high resolution positron emission tomography. IEEE Trans. Nucl. Sci. 2009; 56:182–188.

Fisher RA. The use of multiple measurements in taxonomic problems. Annals of Human Genetics. 1936; 7:179–188.

Ito M, Lee JS, Kwon SI, Lee GS, Hong B, Lee KS, Sim K-S, Lee SJ, Rhee JT, Hong SJ. A four-layer DOI detector with a relative offset for use in an animal PET system. IEEE Trans. Nucl. Sci. 2010; 57:976–981.

Jo JA, Fang Q, Papaioannou T, Marcu L. Fast model-free deconvolution of fluorescence decay for analysis of biological systems. J. Biomed. Opt. 2004; 9:743–752. [PubMed: 15250761]

Krzanowski, WJ. Principles of multivariate analysis : a user's perspective. Oxford Oxfordshire New York: Clarendon Press ; Oxford University Press; 1988.

Li T, Zhu S, Ogihara M. Using discriminant analysis for multi-class classification: an experimental investigation. Knowl. Inf. Syst. 2006; 10:453–472.

Maarek J-MI, Marcu L, Snyder WJ, Grundfest WS. Time-resolved Fluorescence Spectra of Arterial Fluorescent Compounds: Reconstruction with the Laguerre expansion technique. Photochemistry and photobiology. 2000; 71:178–187. [PubMed: 10687392]

Maas MC, Schaart DR, van der Laan DJJ, Bruyndonckx P, Lemaitre C, Beekman FJ, van Eijk CWE. Monolithic scintillator PET detectors with intrinsic depth-of-interaction correction. Phys. Med. Biol. 2009; 54:1893. [PubMed: 19265203]

Marmarelis V. Identification of nonlinear biological systems using laguerre expansions of kernels. Ann. Biomed. Eng. 1993; 21:573–589. [PubMed: 8116911]

Melcher CL, Schweitzer JS. Cerium-doped lutetium oxyorthosilicate - a fast, efficient new scintillator. IEEE Trans. Nucl. Sci. 1992; 39:502–505.

Michaud, J.; Brunet, C.; Lecomte, R.; Fontaine, R. Results from neural networks for recovery of PET triple coincidences; Nuclear Science Symposium Conference Record (NSS/MIC), 2010 IEEE; 2010. p. 3085-3087.

Miyaoka RS, Xiaoli L, Lockhart C, Lewellen TK. Comparison of detector intrinsic spatial resolution characteristics for sensor on the entrance surface and conventional readout designs. IEEE Trans. Nucl. Sci. 2010; 57:990–997. [PubMed: 21614135]

Moses WW, Derenzo SE. Design studies for a PET detector module using a PIN photodiode to measure depth of interaction. IEEE Trans. Nucl. Sci. 1994; 41:1441–1445.

Moses WW, Derenzo SE, Melcher CL, Manente RA. A room temperature LSO/PIN photodiode PET detector module that measures depth of interaction. IEEE Trans. Nucl. Sci. 1995; 42:1085–1089.

Phipps J, Sun Y, Saroufeem R, Hatami N, Fishbein MC, Marcu L. Fluorescence lifetime imaging for the characterization of the biochemical composition of atherosclerotic plaques. J. Biomed. Opt. 2011; 16:096018. [PubMed: 21950932]

Saoudi A, Pepin CM, Dion F, Bentourkia M, Lecomte R, Andreaco M, Casey M, Nutt R, Dautet H. Investigation of depth-of-interaction by pulse shape discrimination in multicrystal detectors read out by avalanche photodiodes. IEEE Trans. Nucl. Sci. 1999; 46:462–467.

Seidel J, Vaquero JJ, Siegel S, Gandler WR, V.Green M. Depth identification accuracy of a three layer phoswich PET detector module. IEEE Trans. Nucl. Sci. 1999; 46:485–490.

St James S, Yang Y, Wu Y, Farrell R, Dokhale P, Shah KS, Cherry SR. Experimental characterization and system simulations of depth of interaction PET detectors using 0.5 mm and 0.7 mm LSO arrays. Phys. Med. Biol. 2009; 54:4605. [PubMed: 19567945]

Tsuda T, Murayama H, Kitamura K, Yamaya T, Yoshida E, Omura T, Kawai H, Inadama N, Orita N. A four-layer depth of interaction detector block for small animal PET. IEEE Trans. Nucl. Sci. 2004; 51:2537–2542.

Wang Y, Seidel J, Tsui BMW, Vaquero JJ, Pomper MG. Performance evaluation of the GE Healthcare eXplore VISTA dual-ring small-animal PET scanner. J. Nucl. Med. 2006; 47:1891–1900. [PubMed: 17079824]

Yang Y, Dokhale PA, Silverman RW, Shah KS, McClish MA, Farrell R, Entine G, Cherry SR. Depth of interaction resolution measurements for a high resolution PET detector using position sensitive avalanche photodiodes. Phys. Med. Biol. 2006; 51:2131–2142. [PubMed: 16625031]

Yang Y, Wu Y, Qi J, James SS, Du H, Dokhale PA, Shah KS, Farrell R, Cherry SR. A prototype PET scanner with DOI-encoding detectors. J. Nucl. Med. 2008; 49:1132–1140. [PubMed: 18552140]

Yousefi S, Lucchese L. Digital pulse shape discrimination in triple-layer phoswich detectors using fuzzy logic. IEEE Trans. Nucl. Sci. 2008; 55:2739–2748.

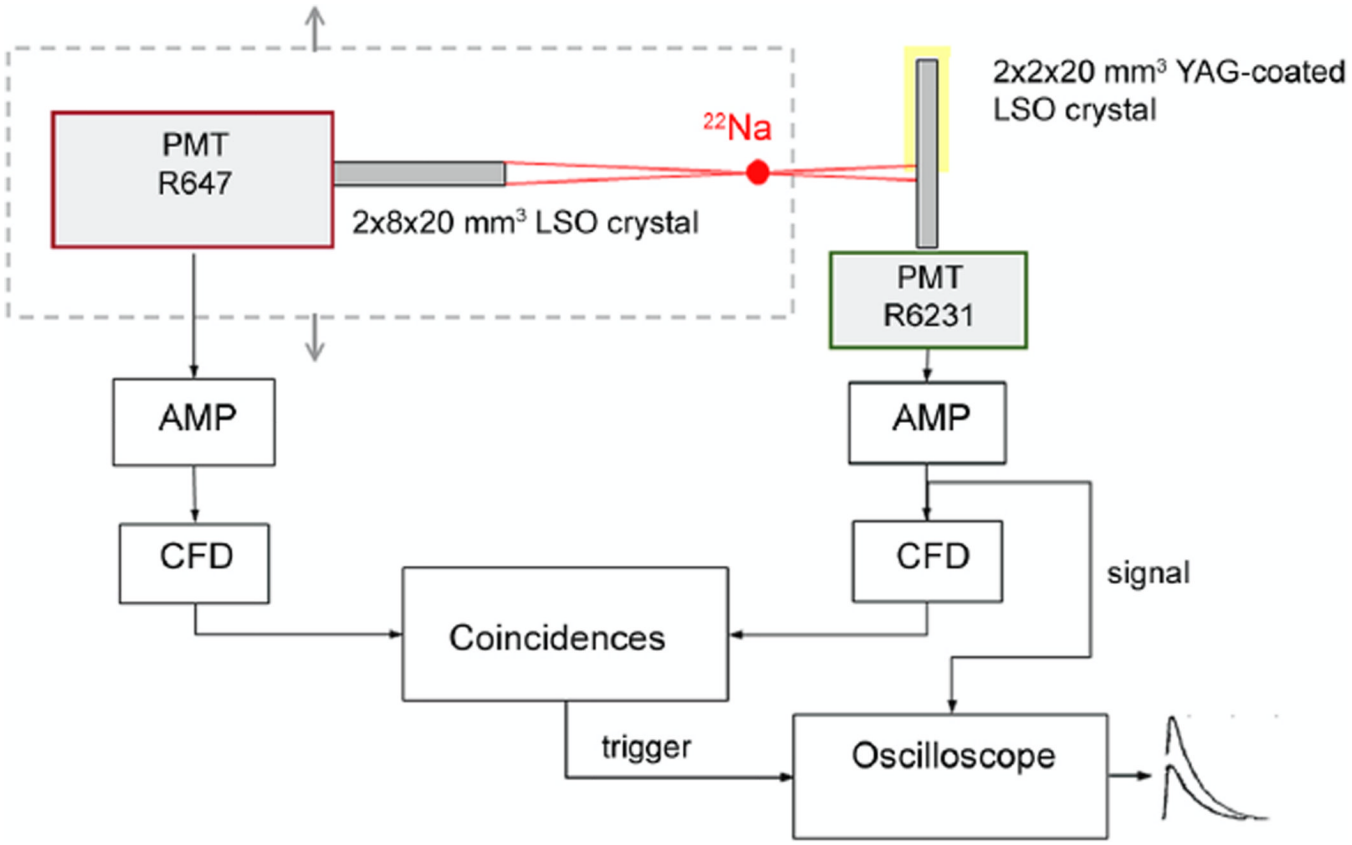


**Figure 1.**
Experimental setup.

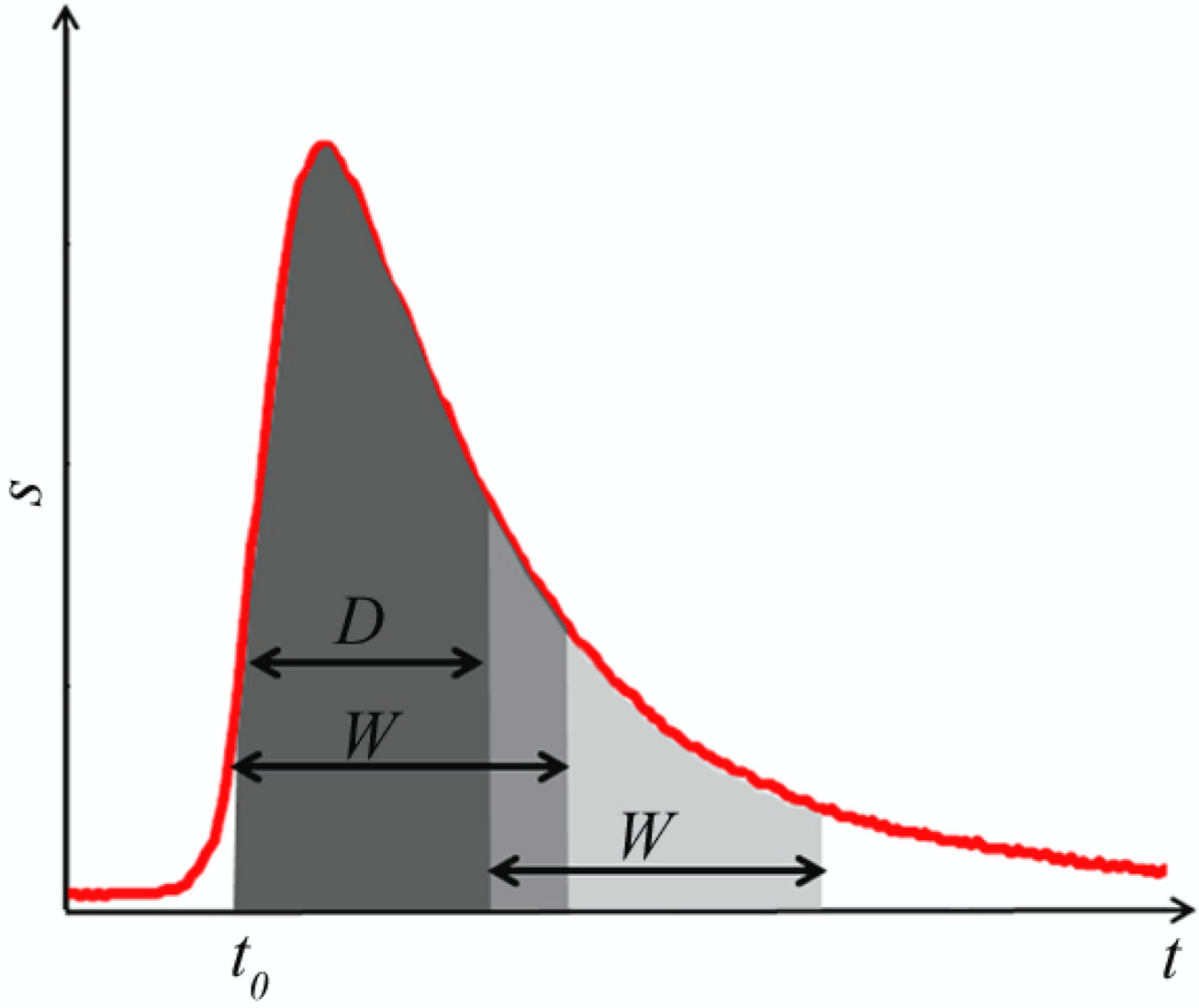


**Figure 2.**
DCI calculation. Two integrals of width *W* are computed at two different starting times ($t_0$ *and* $t_0$+*D*). The DCI value is the ratio of those two integrals.

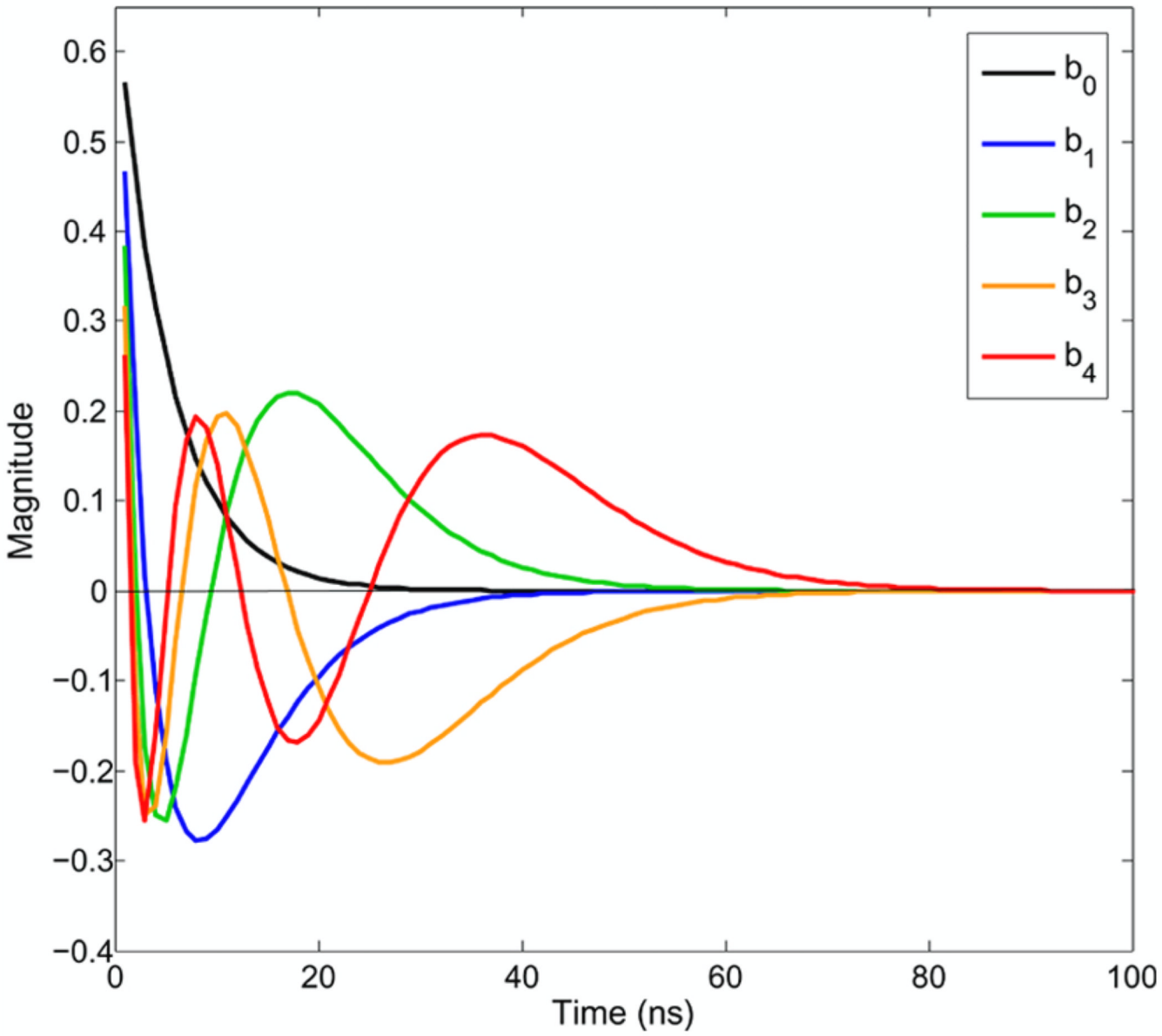


**Figure 3.**
Example of the five first Laguerre basis functions for $I = 8$ and $\alpha = 0.68$ computed from Equation 9.

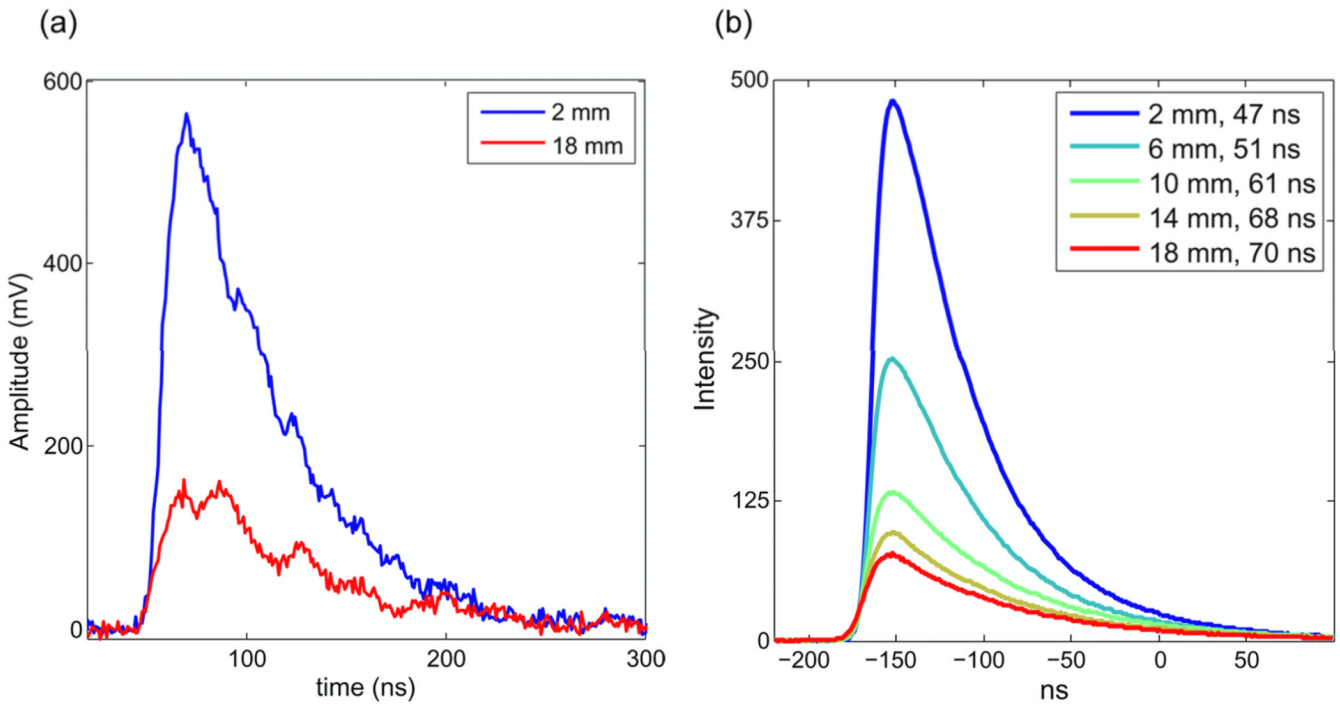


**Figure 4.**
a) Example of individual pulses at 2 mm and 18 mm. b) Averaged pulses measured at each depth. Legend also displays measured decay time for each depth on averaged pulses.

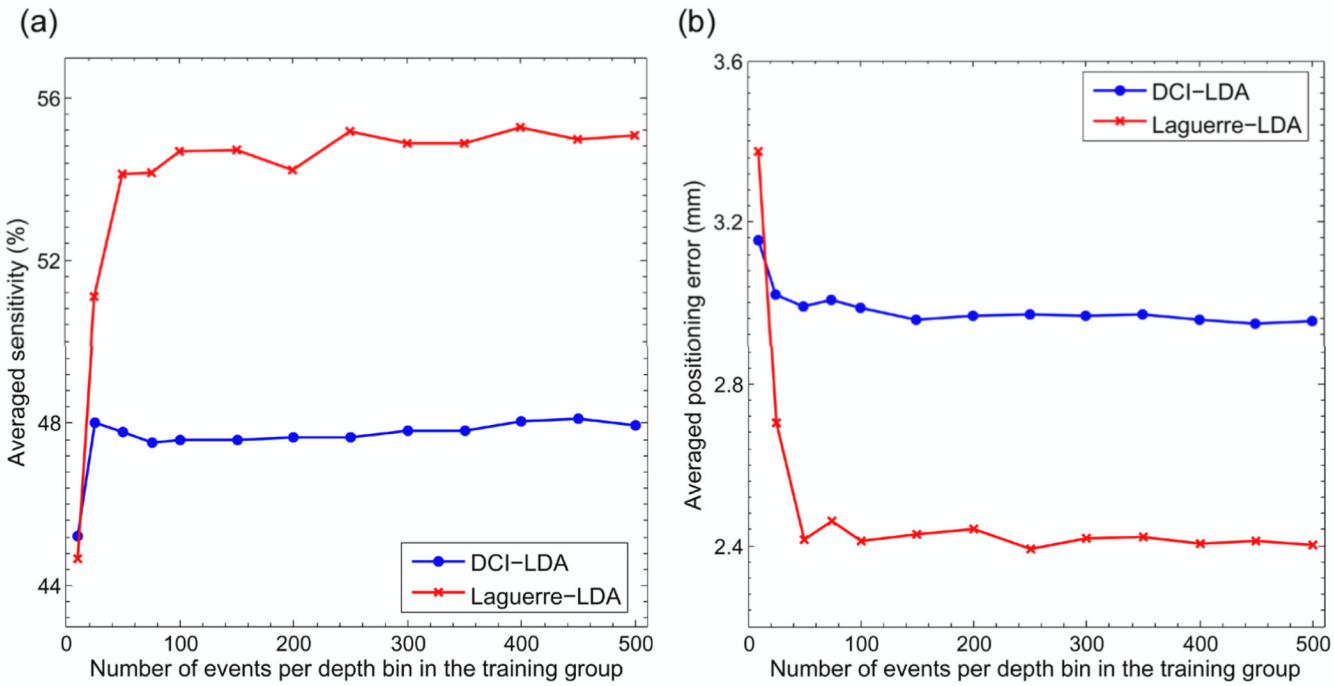


**Figure 5.**
(a) Effect of the training group size on the averaged sensitivity for all bins. (b) Effect of the training group size on the mispositioning of DOI.

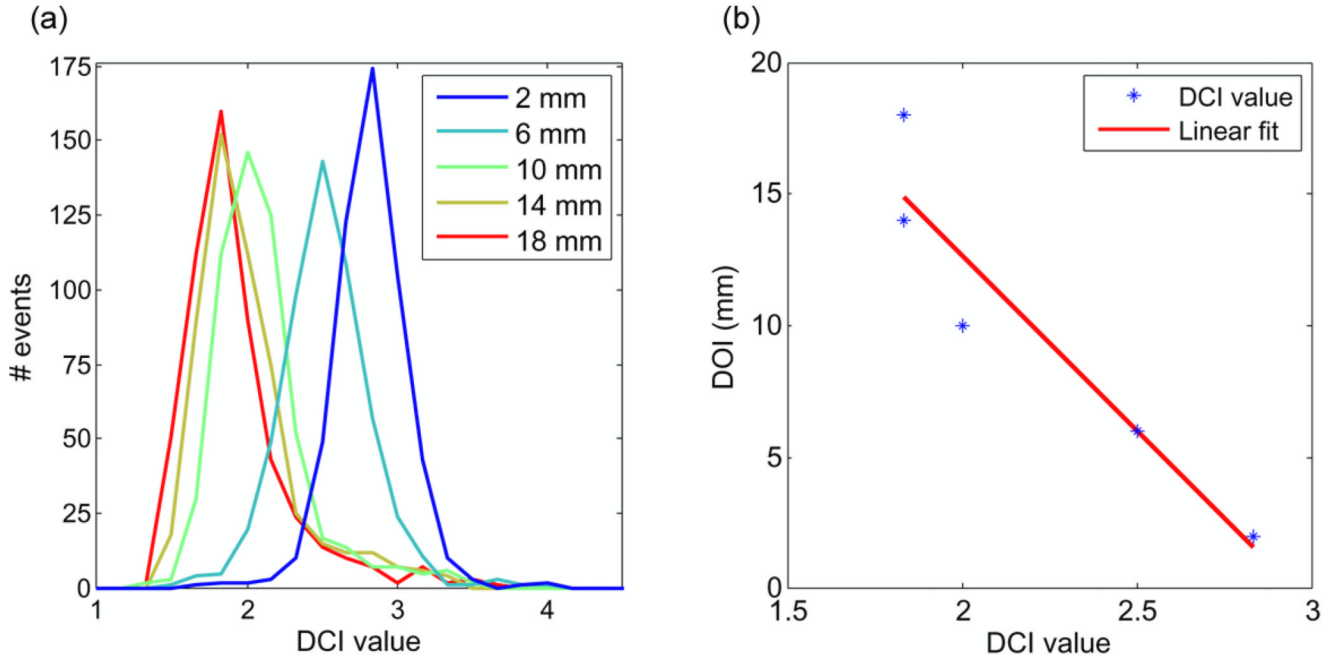


**Figure 6.**
a) Histograms of DCI values for each irradiation depth. b) Known irradiation depth and linear fit plotted against DCI values ($R^2$=0.90).

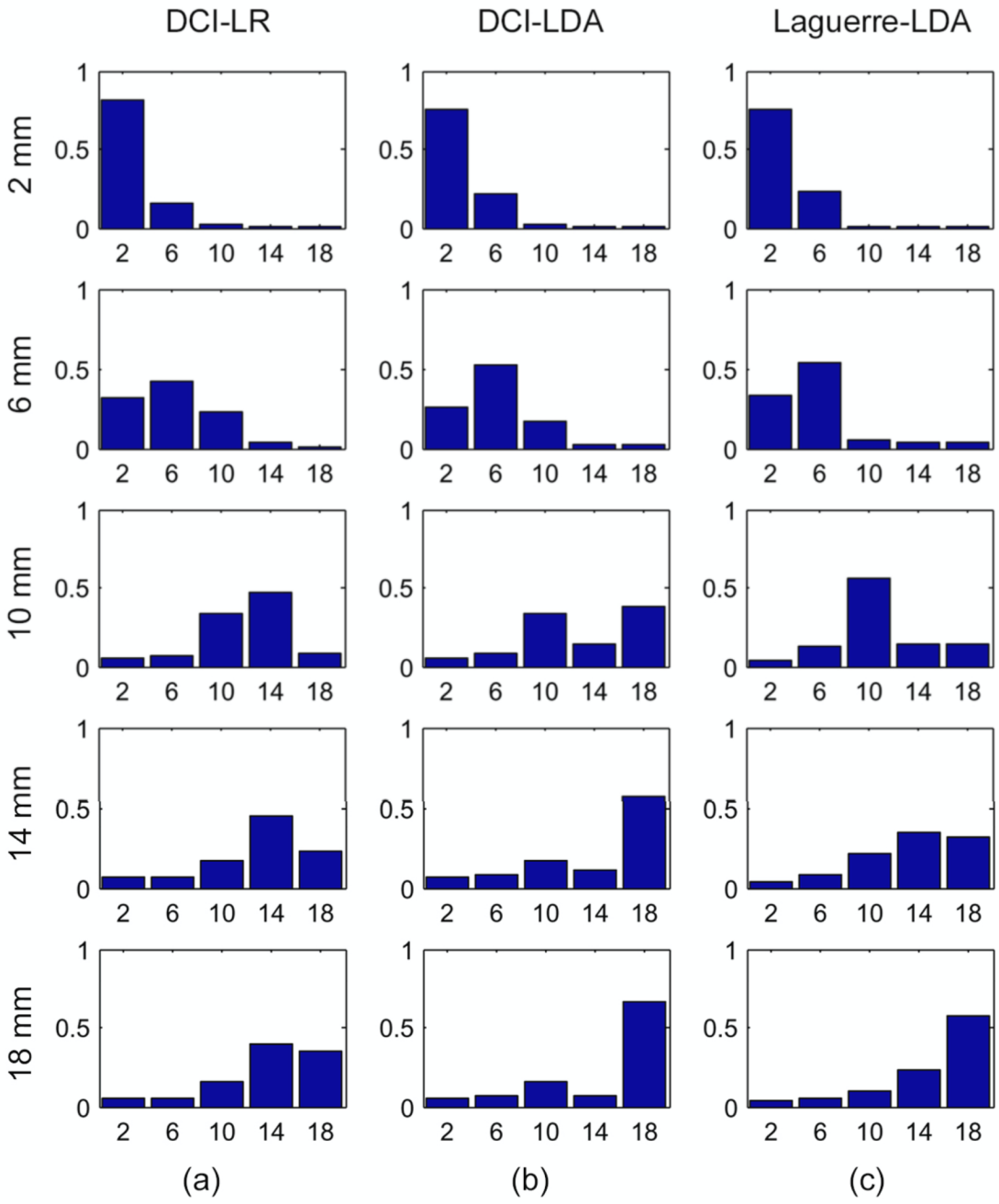


**Figure 7.**

a) Histograms for DCI-LR. b) Histograms for DCI-LDA. c) Histograms for Laguerre-LDA. For all histograms, the x axis shows the depth bins in mm and the y axis displays the fraction of assigned events to those bins. Labels on the left of the plots indicate the irradiation depth (with 2 mm being closest to the photodetector).

**Table 1**

Comparison of sensitivity for all methods.

| DOI Calculation Method | Sensitivity per bin (%) | | | | | Average sensitivity |
|---|---|---|---|---|---|---|
| | 2 mm | 6 mm | 10 mm | 14 mm | 18 mm | |
| DCI-LR | 81 | 41 | 34 | 45 | 35 | 47 |
| DCI-LDA | 76 | 52 | 34 | 11 | 67 | 48 |
| Laguerre-LDA | 75 | 54 | 55 | 35 | 57 | 55 |

**Table 2**

Comparison of positioning error for all methods.

| DOI Calculation Method | Positioning error (mm) | | | | | Average error |
|---|---|---|---|---|---|---|
| | 2 mm | 6 mm | 10 mm | 14 mm | 18 mm | |
| DCI-LR | 0.93 | 2.7 | 3.2 | 2.9 | 4.2 | 2.8 |
| DCI-LDA | 1.1 | 2.3 | 4.3 | 4.2 | 3.0 | 3 |
| Laguerre-LDA | 1.2 | 2.2 | 2.5 | 3.1 | 2.8 | 2.4 |

*Phys Med Biol*. Author manuscript; available in PMC 2013 October 21.